Journal of Mathematical Biology (2026) 92:52
https://doi.org/10.1007/s00285-026-02381-7

Mathematical Biology

Rate-induced tipping in a lake eutrophication model coupled with human activities

Anji Yang[1] · Hao Wang[2] · Sanling Yuan[1]

Received: 11 June 2025 / Revised: 19 January 2026 / Accepted: 8 March 2026

Abstract
Human activities can influence the state of ecosystems, and the consequent variation in ecosystem services in turn affects people's perceptions and behaviors, thus forming a feedback loop. In this paper, a novel coupled human-environment model is proposed and analyzed. The model employs a replicator dynamics equation to describe the human behavioral decision-making process and couples it to an ecological subsystem representing lake eutrophication. Analysis of the model shows that it has richer dynamical behaviors, including multistability and sustained periodic oscillations. Interestingly, for the scenario when the model possesses tristability, we find that increasing the cost of conservation too quickly can trigger rate-induced tipping, causing the system to switch between oligotrophic (or eutrophic) and intermediate steady states. Furthermore, there is a threshold for the rate of change in the cost of conservation below which the probability of tipping from an oligotrophic state to an intermediate nutrient state is always greater than that of switching from an intermediate nutrient state to a eutrophic state. Above this threshold, however, the probability of tipping from the intermediate state to the eutrophic state prevails. Our results suggest that limiting only the magnitude of lake conservation costs is not sufficient to control lake deterioration and that the rate of increase in conservation costs should also be considered.

Keywords Coupled human-environment model · Critical transition · Rate-induced tipping · Tipping probability · Eutrophication of lakes

Mathematics Subject Classification 37N25 · 37B55 · 92B05

✉ Sanling Yuan
sanling@usst.edu.cn

Hao Wang
hao8@ualberta.ca

[1] College of Science, University of Shanghai for Science and Technology, Shanghai 200093, China

[2] Department of Mathematical and Statistical Sciences, University of Alberta, Edmonton AB T6G 2G1, Canada

Published online: 17 March 2026

1 Introduction

Since industrialization at the beginning of the twentieth century, water quality in lakes has worsened, primarily due to anthropogenic factors such as accelerated urbanization (Hall et al. 1999), agricultural production (Bennett et al. 1999), and tourism development (Dokulil 2014). These human activities are often accompanied by releasing compounds such as nitrogen and phosphorus into the natural environment, breaking the balance in the lake ecosystem, and promoting the crazy growth of phytoplankton, with significant negative impacts on biodiversity and human well-being (Carpenter et al. 1999). This process is known as eutrophication, and it is now a global problem; for example, a recent study analyzing nearly three decades of satellite data shows that the problem is worsening in many lakes around the globe (Ho et al. 2019). In the U.S. alone, phosphorus-related water quality problems in the Florida Everglades, Great Lakes, and elsewhere cause more than $2.2 billion in annual economic damages (Dodds et al. 2009). A key factor in successfully managing eutrophication in lakes is the cooperation of multiple parties, such as residents implementing efficient but costly wastewater treatment, the operation of small-scale factories accompanied by decreased phosphorus emissions, and farmers choosing agricultural methods that reduce phosphorus discharges from their fields (Iwasa et al. 2007). In short, managing a eutrophic lake is a complex, multifaceted interaction process between aquatic ecosystems and human subsystems, including social, political, and economic factors (Heggerud et al. 2022). There are noteworthy links between anthropogenic nutrient pollution and eutrophication's economic and ecological consequences.

In previous mathematical models of environmental systems, the effects of human behavior have been represented by constant parameters or functions independent of the current state of the environment (Binford et al. 1987; Carpenter et al. 2017). On shorter time scales, these models do a good job of predicting the optimal level of sustainable resource extraction; however, on longer time scales, human dynamics can change, and it is necessary to include human behaviors in the modeling framework to allow for human-environmental feedback to occur (Heggerud et al. 2022; Liu et al. 2007; Henderson et al. 2016; Bauch et al. 2016; Pananos et al. 2017; Bury et al. 2019). Currently, the study of systems in which human and environmental dynamics are intertwined is beginning to receive more attention. For example, Henderson et al. (Henderson et al. 2016) constructed a nonlinear mathematical model of coupled human-environment dynamics in forest-grassland mosaic systems and social processes about conservation and economic land valuation. They found that the mosaic is currently at a crucial moment where relatively minor changes in social conditions can produce a variety of possible outcomes. Bury et al. (Bury et al. 2019) linked dynamic social processes associated with greenhouse gas emissions to climate models for understanding how social and climate processes interact. The problem of early warning signals for critical transitions in coupled human-environment systems was investigated by Bauch et al. (Bauch et al. 2016). In addition, human behavioral dynamics are integrated with other common-pool resource systems, such as fisheries, to understand the trade-offs between profit-seekers and sustainable resource usage (Sarkar et al. 2021). There are also studies that utilize social processes to provide insights into disease outbreaks (Pananos et al. 2017; Bauch 2005; Oraby et al. 2014). For lake ecosystems, the coupled dynam-

ics of people's socio-economic decisions and lake nutrient balance were investigated by Iwasa et al. (Iwasa et al. 2007, 2010). Based on this modeling idea, Heggerud et al. (Heggerud et al. 2022) considered phytoplankton dynamics in the coupled system, and the results showed that the coupled model has a bistable regime, where one steady state corresponds to high abatement effort and low algal biomass, and the other steady state corresponds to low abatement effort and high algal biomass. In Ref. Sun and Hilker (2020), Sun et al. used the best-response dynamics to portray human behavior and combined it into a generic model of eutrophication, and they found that the coupled model could have up to four stable equilibrium points. In this paper, we will use the replicator dynamics equation to inscribe human behavioral decision-making processes and couple it to an ecological subsystem representing lake eutrophication (Farahbakhsh et al. 2022). Both the replicator and the best-response dynamics come from evolutionary game theory and describe the evolution of the collective choice of individuals between different strategies at a population level. Hopkins (Hopkins 1999) proved that the best-response dynamics can be understood as a perturbed version of a generalized replicator dynamics.

Coupled human-environment systems are often characterized by strong nonlinearities and may exhibit complex dynamical behaviors such as the coexistence of multiple attractors (including equilibria and limit cycles) as well as numerous global bifurcation phenomena (Farahbakhsh et al. 2022; Mandal et al. 2025). Such nonlinear dynamical systems are prone to trigger regime shifts (also known as critical transitions), which means that the system suddenly shifts from its current state to a significantly different state when the external conditions surpass a tipping point (Scheffer et al. 2009). The theory of nonlinear dynamics has significantly improved our knowledge of certain types of tipping points. For example, the type of regime shift that occurs when external conditions exceed a critical level or a dangerous bifurcation point is referred to as bifurcation-induced tipping (B-tipping), which manifests itself as the steady state loses stability or simply disappears (Scheffer et al. 2009; Kuehn 2013; Dai et al. 2012; Wang et al. 2012). The second type of tipping point, due to regime shifts induced by larger random perturbations in systems with alternative steady states, is known as noise-induced tipping (N-tipping) (Yang et al. 2022; Boettiger 2018; Yang et al. 2023, 2024; Ma et al. 2019).

Unfortunately, the B-tipping and N-tipping theories are based on the assumption of equilibrium dynamics and do not resolve regime shifts induced solely by the rate of parameter change (Siteur et al. 2016; O'Keeffe and Wieczorek 2020; Lohmann and Ditlevsen 2021). In fact, rate-induced tipping (R-tipping) occurs when the parameter change rate is faster than some critical rate such that the trajectory deviates far enough from the moving equilibrium state to cross the boundary of the basin of attraction (Ashwin et al. 2017). In recent years, research on rate-induced tipping has attracted widespread attention from more and more scholars. For example, Wieczorek et al. (Wieczorek et al. 2023) establish an accessible mathematical framework for R-tipping in multidimensional nonautonomous dynamical systems with an autonomous future limit. For one-dimensional systems, Ashwin et al. (Ashwin et al. 2017) proposed the concept of forward basin stability and utilized this to give sufficient conditions for the occurrence of rate-induced tipping. For higher dimensional systems, Kiers et al. (Kiers and Jones 2020) argue that forward inflowing stability is sufficient to prevent R-tipping.

In actual ecosystems, Gil et al. (Gil et al. 2020) found that increasing fishing rapidly to a certain level could collapse an ecosystem, while under more gradual changes the ecosystem would persist. To our knowledge, current coupled human-environment models almost always assume constant parameters related to the social and ecology subsystem, e.g., fixing the net cost of pollution mitigation (Sun and Hilker 2020). However, as society develops, the pursuit of economic gain will inevitably increase the nutrient loading of lakes, and the cost of protecting them is likely to increase significantly in both time and money. The research in this paper will focus on rate-induced tipping to understand the effect of the rate of change of system parameters on lake nutrient levels.

The organization of this paper is as follows. In Sect. 2, we develop a socio-ecological model of lake pollution, where individuals in the group either choose to hold a protective attitude toward the environment to reduce the pollution rate or betray it by continuing to pollute the environment at a higher rate. We perform a basic analysis in Sect. 3 on the dynamics of the coupled model, including the existence and stability of equilibrium. In Sect. 4, we begin with the simplest dynamics regime with no coupling between the ecological and social subsystems and then investigate the complex dynamics that result when the two subsystems are coupled. The results of the bifurcation analysis show that a change in the magnitude of the conservation cost will lead to a variety of dynamical regimes in the coupled system, including monostability, bistability, and tristability. We then focus our attention on the tristability scenario, when the system has three stable attractors corresponding to the oligotrophic, intermediate, and eutrophic states. In Sect. 5, we first give the theoretical framework needed to characterize rate-induced tipping and introduce the notion of basin instability associated with the initial states. The cost of conservation is then treated as a linear growth function, exploring the effect of the rate of increase in w on lake nutrient levels as well as on the basins of attraction of the three attractors. To evaluate rate-tipping risk, we introduce the notion of rate-tipping probability and give a detailed numerical calculation process. Finally, we conclude our study by a brief discussion in Sect. 6.

2 Model formulation

2.1 Environment dynamics model

In terms of ecological dynamics, we use a stylized lake eutrophication model to describe the nutrient (phosphorus) dynamics of shallow lake ecosystems. We built on this basic model because it is a relatively simple and well-studied model in the lake ecosystem, and can well represent the trophic state of lake ecosystems according to phosphorus loading rates. In addition, the model has been successfully applied to the eutrophication management of Lake Mendota, Wisconsin (Carpenter et al. 1999). Thus, the model is a stepping stone to understanding more complex coupled systems involving multiple factors. The model is defined as follows:

$$\frac{\mathrm{d}P}{\mathrm{d}t} = \underbrace{\alpha}_{\substack{\text{anthropogenic emissions}\\ \text{of phosphorus}}} + \underbrace{\frac{rP^q}{m^q + P^q}}_{\text{resuspension}} - \underbrace{hP}_{\text{loss term}}, \tag{1}$$

where variable P represents the phosphorus concentration in lake water at time t. The model assumes a fixed phosphorus input rate α, which is dominated by point sources (e.g. industrial or municipal sewage discharge) and non-point source (e.g. agricultural or urban runoff) pollutants from the watershed. On the other hand, a large portion of the available phosphorus pool in shallow lakes exists in sediments (Scheffer et al. 1998). Therefore, phosphorus can be recirculated from the sediment into the lake water after disturbance by waves or fish. Although phosphorus can also be recycled by consumers, here we will assume that sediment is the main source of recycled phosphorus. According to Ref. (Carpenter et al. 1999), the second item in the environmental subsystem (1) represents the phosphorus resuspension process. It follows a sigmoid-shaped curve, where m is the half-saturation level and r is the maximum recycling rate. The parameter q, which reflects the steepness of this curve (larger values of q give a steeper curve), is negatively correlated with the depth of the lake and takes values in the range [2, 20]. Larger values of q are recommended for shallow and warm lakes, when a steeper internal phosphorus circulation slope makes the shallow lake more likely to produce alternative steady states, whereas for deep and cold lakes, the parameter q should be relatively small. Here we set q equal to 2. The loss of phosphorus in lakes primarily includes outflow, deposition, and sequestration within phytoplankton or aquatic plants, which is proportional to the concentration of phosphorus in the lake water. h is the phosphorus loss rate.

2.2 Social dynamics model

Note that in model (1) human behavior is characterized by a constant rate of phosphorus input α, so this is not a coupled human-environment system. In fact, social behavior is not static and changes depending on how people perceive the state of the ecosystem. In order to elucidate social dynamics, we employ imitation dynamics within the framework of evolutionary game theory, which encapsulates the tendency of humans to emulate successful strategies (Lade et al. 2013; Bauch 2005). The population is assumed to be divided into two groups only, where x represents the proportion of people who adopt viewpoint C ('conservationists'), i.e., support the reduction of phosphorus runoff to maintain lake ecosystem services. In contrast, the remaining proportion $1 - x$ adopts viewpoint NC ('non-conservationists'), i.e., those who support activities such as agriculture, forestry, and urban development to maximize economic benefits, but these polluting activities promote phosphorus inputs. Each individual in the population takes one of the two views. Each individual's choice will be influenced by the "utility" associated with the two perspectives, which quantifies the popularity of the corresponding perspective (Fishburn 1970).

Assume that individuals randomly sample the other members of the population at some constant rate. If the sampled member has the contrary view and offers a higher utility, then the individual shifts to the sampled member's view with a probability

proportional to the expected gain in utility. The proportion x of lake conservationists can reduce by individuals shifting from C to NC or increase by individuals shifting from NC to C. A NC individual sampling at rate k encounters C individuals with frequency kx and observes the utility gain for shifting opinions is $\Delta G = G_C - G_{NC} > 0$. Here G_C and G_{NC} represent the utility associated with holding opinions C and NC, respectively. Considering that there are $1-x$ NC individuals in the population, the total rate of individuals shifting from NC to C is $(1-x)\cdot kx \cdot [G_C - G_{NC}] = kx(1-x)\Delta G$. Similarly if $G_{NC} - G_C > 0$ then the total rate of individuals shifting from C to NC is $x \cdot k(1-x) \cdot [G_{NC} - G_C] = -kx(1-x)\Delta G$. Accordingly, the time evolution of the proportion of lake conservationists x is described as

$$\frac{\mathrm{d}x}{\mathrm{d}t} = kx(1-x)\Delta G - (-kx(1-x)\Delta G) = \kappa x(1-x)\Delta G, \tag{2}$$

where $\kappa = 2k$ is the social learning rate. The state variable x indicates the fraction of individuals in the population who support the conservation of the environment and therefore ranges from 0 to 1. When x is relatively small, we call it a low level of conservationists in the population; analogously, when x is relatively large, we call it a high level of conservationists in the population. Obviously, here we use the replicator dynamics equation to represent the social process (Smith 1982). Our choice of replicator dynamics is based on the assumption that individuals are perfectly rational and always choose the opinion that is more beneficial to them (Hofbauer and Sigmund 2003). Furthermore, this social dynamics model has two equilibria: if $G_C - G_{NC} > 0$ (i.e., $\Delta G > 0$), then opinion C ('conservationists') prevails in the population; conversely, if $G_{NC} - G_C > 0$ (i.e., $\Delta G < 0$), then opinion NC ('non-conservationists') is the majority in the population.

2.3 Coupled human-environment model

Human activities can influence the state of ecosystems, and the consequent variation in ecosystem services in turn affects people's perceptions and behaviors, creating a feedback loop that often changes the path of ecosystems back to their natural state (Liu et al. 2007; Galvani et al. 2016). Therefore, natural ecosystems and human systems should be conceptualized as a coupled human-environment system.

For the uncoupled environmental model (1), the anthropogenic phosphorus input rate is set as a constant α. However, in the coupled human-environment model, the phosphorus input rate should be a function related to the human state variable x. Hence, it is necessary to modify the term anthropogenic emissions of phosphorus in Eq. (1). Likewise, ΔG should not be a fixed parameter, but change with phosphorus concentration. Specifically, the utility difference ΔG between viewpoints C and NC is taken in such a form that, when the nutrient level P of the lake is too high, the utility of continuing to discharge pollutants decreases, thus making more individuals take a protectionist view. In turn, when natural resource conservationist opinions dominate in the population, phosphorus input rates decrease.

We define a payoff structure for pairwise interactions between two strategies, where the payoff matrix is environment-dependent (Weitz et al. 2016):

$$A(P) = \begin{bmatrix} \delta - w & -w \\ -P & -P + \delta \end{bmatrix}. \tag{3}$$

The payoff-dependent fitnesses can be written as follows:

$$G_C = -w + \delta x, \quad G_{NC} = -P + \delta(1 - x).$$

Therefore, the utility difference ΔG has the following form:

$$\Delta G = -\underbrace{w}_{\text{conservation costs}} + \underbrace{P}_{\text{ecological concern}} + \underbrace{\delta(2x - 1)}_{\text{social norms}}. \tag{4}$$

Next, we discuss in detail the three factors that influence the difference in utility ΔG:

(i) **Conservation costs:** w is called mitigation costs (or conservation costs) and includes both monetary costs and non-monetary costs, such as time costs. If the mitigation cost is too high, it will attenuate lake protection.
(ii) **Ecological concern:** The degree of individual concern for the ecosystem is positively correlated with the nutrient level of the lake. If the phosphorus concentration in lake water increases, more individuals tend to conserve (cooperate) in reducing the rate of phosphorus input.
(iii) **Social norms:** δ represents the magnitude of injunctive social norms that propel individuals toward the prevailing opinion held by the majority of the population. For instance, the more conservationists there are, the more people tend to protect the environment.

We substitute formula (4) into Eq.(2), and then combine environmental system (1) with human system (2) to obtain a comprehensive model

$$\begin{aligned} \frac{\mathrm{d}P}{\mathrm{d}t} &= \alpha(1 - x) + \frac{rP^2}{m^2 + P^2} - hP, \\ \frac{\mathrm{d}x}{\mathrm{d}t} &= \kappa x(1 - x)\left[-w + P + \delta(2x - 1)\right]. \end{aligned} \tag{5}$$

All parameters of the model are positive, and the interpretation of the parameters is tabulated in Table 2. Note that model (5) assumes that the effect of human behavior on phosphorus runoff is represented by the $\alpha(1 - x)$ term. Thus, the most fundamental advantage of this coupled model is its potential to capture the dynamics in a system where humans and the environment respond to each other, which is an increasingly common scenario in the context of global warming.

Table 1 Boundary dynamics of model (5) when $x = 1$

Equilibrium	Existence condition	Stability condition
E_{01}	Always	Sink if $w < \delta$; Saddle if $w > \delta$.
E_{11}	$r > 2hm$	Saddle whenever it exists.
E_{21}	$r > 2hm$	Sink if $w < \delta$; Saddle if $w - \delta > P_{21}$.

3 Model analysis

In this section, we investigate the dynamics of model (5). Since model (5) portrays the feedback dynamics between lake phosphorus concentrations and the proportion of conservationists in the population, we first show that model (5) is biologically well-defined.

Lemma 1 *Model (5) is positively invariant in $\mathbb{R}^2_+$, and for any given initial value $(P(0), x(0)) \in \mathbb{R}^2_+$, the solution $(P(t), x(t))$ will eventually be attracted to the positive invariant set*

$$\Omega = \left\{ (P, x) \in \mathbb{R}^2_+ : 0 \le P \le \frac{\alpha + r}{h}, 0 \le x \le 1 \right\}.$$

In the following analysis, we need only consider the dynamics of model (1) on the region Ω. The shape of nullclines is crucial for the occurrence of complex dynamics (e.g., oscillations or multistability). Also, to obtain analytic conditions for the basic dynamics of the deterministic model (5), including the number of equilibrium and stability, we summarize below the composition of the x-nullcline in the social subsystem. From the second equation in model (5) for the variable x, the x-nullcline consists of three parts: (i) $x = 1$ and $P > w - \delta$, when the population is full conservationism; (ii) $x = 0$ and $P < w + \delta$, implying no conservationism in the population; (iii) $\Delta G = 0$ and $0 < x < 1$, which is a straight line in the phase plane with equation $x = -\frac{1}{2\delta}P + \frac{w+\delta}{2\delta}$. In the following, we analyze the boundary dynamics of model (5) at $x = 1$ or 0 and the interior equilibrium dynamics of the model at $\Delta G = 0$, respectively.

3.1 Dynamics of boundary equilibria

Theorem 1 (Boundary dynamics when $x = 1$) *Model (5) always has equilibrium $E_{01} = (0, 1)$, representing the oligotrophic state. In addition, when $r > 2hm$, model (5) possesses two boundary equilibria $E_{11} = (\frac{r-\sqrt{r^2-4h^2m^2}}{2h}, 1)$ and $E_{21} = (\frac{r+\sqrt{r^2-4h^2m^2}}{2h}, 1)$. Threshold conditions for the boundary dynamics when $x = 1$ are summarized in Table 1.*

Theorem 2 (Boundary dynamics when $x = 0$) *If $r > 8\alpha$, model (5) may have from one to three boundary equilibria. Moreover,*

(i) If $\beta(P_-) < h < \beta(P_+)$, model (5) has three boundary equilibria $E_{i0} = (P_{i0}, 0)$, $i = 1, 2, 3$, with $P_{10} < P_{20} < P_{30}$, then E_{10} and E_{30} are locally asymptotically stable (LAS), and E_{20} is unstable.

(ii) If $h < \beta(P_-)$ (or $h > \beta(P_+)$), model (5) has a unique boundary equilibrium E_{30} (or E_{10}), then E_{30} (or E_{10}) is LAS.

(iii) If $h = \beta(P_-)$ (or $h = \beta(P_+)$), model (5) has two boundary equilibria in which one is a double equilibrium, then the double equilibrium is a saddle-node and the other is LAS.

The proofs of Theorems 1 and 2 are given in Appendices A and B, respectively. According to these two theorems, the boundary steady state $E_{30} = (P_{30}, 0)$ (or $E_{01} = (0, 1)$) is locally asymptotically stable if $\delta > P_{30} - w$ (or $\delta > w$). Therefore, depending on the environmental parameters, increasing the strength of social norms δ tends to push the population towards the extremes of full conservationism ($x = 1$) or no conservationism ($x = 0$). For example, as in Figs. 1 (A)-(B), at relatively low conservation costs and nutrient input rates, increasing the strength of social norms can destabilize internal oscillations and lead to a regime shift to a state of no-phosphorus emissions and complete conservationism. The corresponding undesirable state of high phosphorus concentrations and non-conservationism is unstable at these parameter values. At higher phosphorus input rates, the fold bifurcation moves to the right and the parameter region corresponding to its stable lower branch decreases, while the range of the parameter region corresponding to the stable limit cycle gradually expands (see Figs. 1 (C)-(D)).

3.2 Dynamics of interior equilibria

In this subsection, we will employ δ and m as control parameters to discuss the number and stability of interior equilibria where the proportion of conservationists is non-zero but less than 1. For the existence and stability of interior equilibria, we have the following theorem. The proof of Theorem 3 is in Appendix C.

Theorem 3 (Interior dynamics when $0 < x < 1$) *If $r < 4\alpha$, $w < \delta < \delta^*$, model (5) can have up to three interior equilibria. Moreover,*

(i) If $m^- < m < m^+$, model (5) has three distinct interior equilibria denoted, respectively, by $E_i = (P_i, x_i)$, $i = 1, 2, 3$, with $P_1 < P_2 < P_3$, then E_1 and E_3 are unstable, and E_2 is LAS.

(ii) If $m = m^-$ (or $m = m^+$), model (5) has two interior equilibria, both of which are unstable.

(iii) If $m < m^-$ (or $m > m^+$), model (5) has a unique interior equilibrium, denoted by $E_* = (P_*, x_*)$, then E_* is LAS provided $K_2 < K_1 < 0$ and $K_1 + \overline{K} < 0$ are satisfied, where $K_i = f_i'(P_*)$, $i = 1, 2$ and $\overline{K} = 2\kappa\delta x_*(1 - x_*)$.

In the next section, we will review the basic dynamics of the uncoupled model (1), which is equivalent to the case where the x-variable is 0 in the coupled model, i.e., there are no conservationists in the population. The bifurcation analysis can provide valuable insights into the system's dynamics and the existence of different equilibria. We then focus on the richer dynamics of the coupled model (5) through bifurcation diagrams. The model parameter values are taken from Table 2.

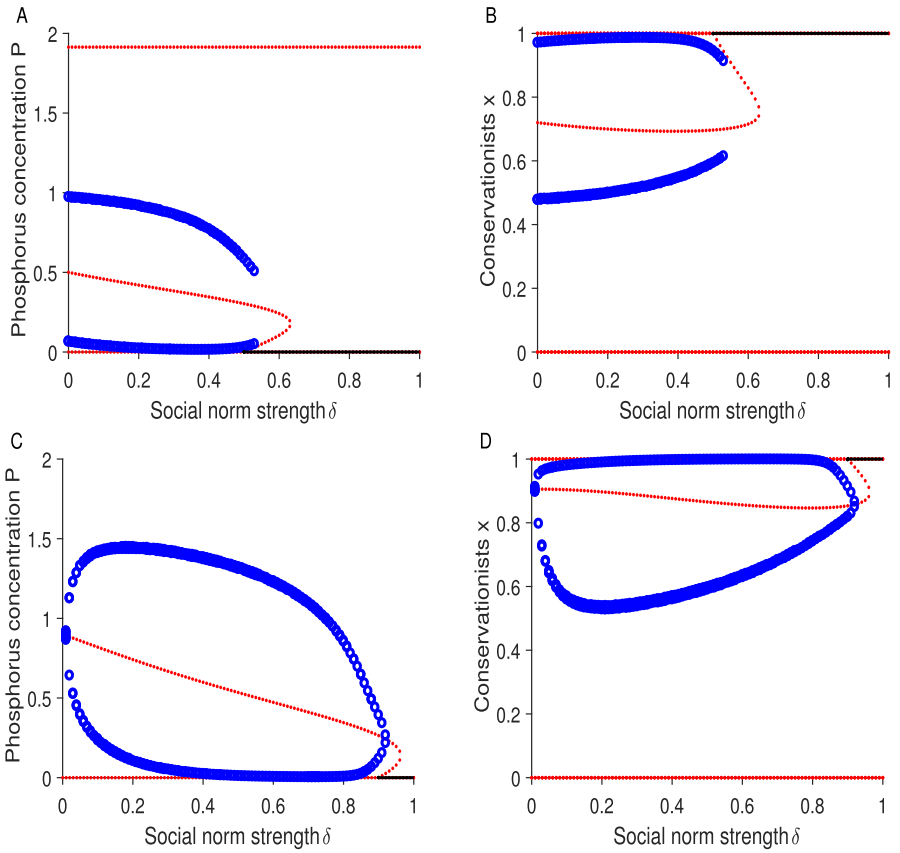

Fig. 1 Bifurcation diagrams of model (5) versus social norm strength (δ) for distinct values of the conservation cost (w) and input rate of phosphorus (α). (A and B) $w = 0.5$, $\alpha = 0.5$ and (C and D) $w = 0.9$, $\alpha = 1$. The solid black line represents the stable equilibrium, the red dashed line represents the unstable equilibrium, and the blue cycle is the amplitude of the limit cycle. Other parameter values are as in Table 2

Table 2 Interpretations and baseline values of parameters for coupled human-environment system (5)

Parameter	Description	Value (Range)	Units	Sources
κ	The social learning rate	1	y^{-1}	Default
w	Conservation costs	0.9	Unitless	Default
δ	Social norm strength	1	Unitless	Default
α	Input rate of phosphorus	1	$g \cdot m^{-2} \cdot y^{-1}$	Carpenter et al. (1999)
h	Loss rate of phosphorus	1	y^{-1}	Carpenter et al. (1999)
r	Maximum recycling rate of phosphorus	[0, 3.65]	$g \cdot m^{-2} \cdot y^{-1}$	Genkai-Kato et al. (2012)
m	The half-saturation constant	1	$g \cdot m^{-2}$	Suzuki and Iwasa (2009)

4 Dynamical regimes

4.1 Basic dynamics of the uncoupled model

From Theorem 2 we know that the number of steady states in the ecological subsystem depends on the rate of phosphorus input and the intensity of nutrient losses. When $\alpha < \frac{r}{8}$, model (1) has at least one steady state and at most three equilibria. For a suitable phosphorus input rate, this model possesses two stable equilibria corresponding to the oligotrophic and eutrophic states, and one unstable equilibrium. In addition, this model can demonstrate a regime shift, i.e., the typical dynamics that occurs in many ecological models. Regime shifts can be well understood through bifurcation diagrams, which visualize the steady state position of the system and how the number of equilibrium points and stability vary with model parameters (Drazin 1992). A bifurcation occurs when the stability of an equilibrium state changes, often due to "collision" with another equilibrium. In a bifurcation plot of phosphorus concentration P versus phosphorus input rate α, we observe that the lake is persistently in an oligotrophic state when the phosphorus input rate is low. When α is large enough a tipping point is encountered and a regime shift occurs. The unstable state collides with the oligotrophic state, leaving only the stable eutrophic state. This bifurcation diagram, not shown in this article, is similar to Fig. 2 (A). This type of tipping mechanism is called Bifurcation-induced tipping and corresponds to the collision and annihilation of stable and unstable equilibria.

4.2 Complex dynamics of the coupled model

We investigate the dynamics of model (5) by varying the coupled system parameters. Also, model parameters are taken from Table 2 unless otherwise stated. For some parameter values, the results of the coupled human-environment model are similar to those of the uncoupled model. For example, when the cost of conservation is sufficiently high ($w = 0.9$) and the social norm is sufficiently strong ($\delta = 1$), the lake stabilizes in a eutrophic state as the phosphorus input rate α increases (Fig. 2 (A)). A sufficiently strong social norm polarizes attitudes in the population, i.e., either fully conservationist ($x = 1$) or no conservationist ($x = 0$). But the no conservationist state corresponds to a much larger basin of attraction (Fig. 2 (B)). Thus, in the case of excessively high conservation costs, injunctive social norms make it difficult for protectionism to take root in the population.

However, this similarity to the uncoupled model does not hold in general. Although excessive nutrient inputs are certainly the direct cause of eutrophication in lakes, from the perspective of human-environment coupling, nutrient inputs are only the final result of the interaction between economic, social, and ecological factors. For example, if the social norm is weak ($\delta = 0.1$) and the cost of conservation is low ($w = 0.2$), a very distinct result emerges: as the rate of nutrient inputs exceeds a tipping point, the human response to lake eutrophication is to increase conservationism, i.e., $x > 0$ becomes stable in Fig. 2 (D). This, in turn, permits nutrient concentrations in the lake to remain moderately low in the face of high nutrient input rates (Fig. 2 (C)). Compared

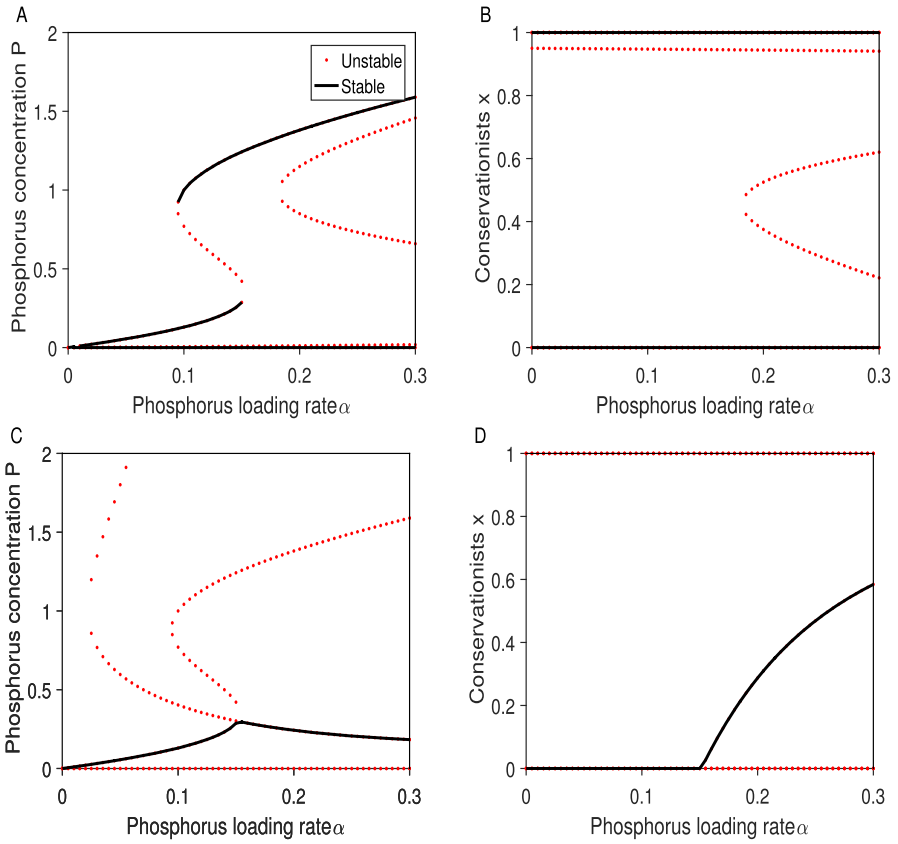

Fig. 2 Bifurcation diagrams depict the rich diversity of regimes in the coupled human-environment model (5), such as (**A** and **B**) leading to eutrophication through saddle-node bifurcation and (**C** and **D**) leading to conservation scenarios through transcritical bifurcation. Shown are (**A** and **C**) phosphorus concentration P and (**B** and **D**) conservationists x, vs. loading rate α for (**A** and **B**) $w = 0.9$, $\delta = 1$ and (C and D) $w = 0.2$, $\delta = 0.1$. The solid black line represents the stable equilibrium, and the red dashed line represents the unstable equilibrium. Other parameter values are as in Table 2

to the uncoupled model, the population in the coupled model responds to the threat of eutrophication of the lake due to excessive input rates by limiting nutrient inputs, thus allowing the lake's nutrients to be maintained at relatively low levels. Recall from the mathematical model that the input rate is given by $\alpha(1 - x)$, so when x grows fast enough, the nutrient input is limited despite the high values of α.

As shown previously, coupled human-environment models exhibit richer dynamical behavior than uncoupled models. Outcomes such as lake eutrophication may rely on complicated interactions between model parameters, which can be understood through bifurcation plots involving other model parameters. Fig. 3 shows the bifurcation diagrams of phosphorus concentration (P) versus conservation cost (w) for various values of the social norm strength (δ). As the cost of conservation w increases, the no-phosphorus-emission and full conservationism, $(P, x) = (0, 1)$,

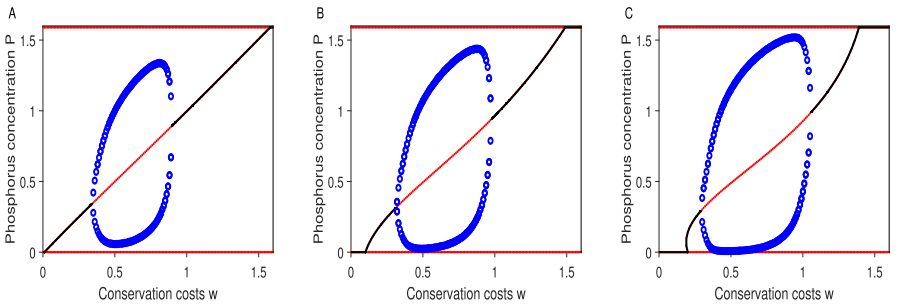

Fig. 3 Bifurcation diagrams of phosphorus concentration (P) versus conservation cost (w) for various values of the social norm strength (δ): (**A**) $\delta = 0.01$, (**B**) $\delta = 0.1$, (**C**) $\delta = 0.2$. Increasing the social norm intensity helps to increase the trend and amplitude of the oscillations. The solid black line represents the stable equilibrium, the red dashed line represents the unstable equilibrium, and the blue cycle is the amplitude of the limit cycle. The phosphorus input rate (α) is taken as 0.3, and the other parameters values are shown in Table 2

can be replaced by full non-conservationism with maximal phosphorus emissions. Local stability analyses also reflect this result: The $(P, x) = (0, 1)$ equilibrium is locally asymptotically stable when $w < \delta$, indicating that weak social norms and high conservation costs can destabilize non-phosphorus emissions and conservationism. Interestingly, the phosphorus input rate parameter α in ecosystems does not appear in this condition. Moreover, for a suitable w, the limit cycle may appear and the coupled model enters a regime of stable oscillations in public opinion and phosphorus concentration. As phosphorus concentrations increase, public opinion shifts in favor of protectionism, which contributes to a decline in phosphorus emissions. This in turn leads to a decline in conservationism and the cycle continues. The bifurcation diagram also shows that increasing the social norm intensity δ destabilizes the system by expanding the range of values of w for which oscillatory solutions are acquired. Additionally, increasing the social norm intensity helps to increase the trend and amplitude of the oscillations.

Although larger social norm strengths may trigger a limit cycle in the system, by analyzing the local stability of the internal equilibrium, we find that one of the conditions for $E_* = (P_*, x_*)$ to be stable is that the social learning rate κ needs to be small, i.e., $\kappa < \frac{h(m^2+P_*^2)^2-2rm^2P_*}{2\delta x_*(1-x_*)(m^2+P_*^2)^2}$. We take a relatively small value for the social learning rate, i.e., $\kappa = 0.2$, and show in Fig. 4 (A) a two-parameter bifurcation diagram in the (w, δ) plane and (B) a one-parameter bifurcation diagram of the conservationist variable x with respect to the conservation cost w for model (5). The two-parameter bifurcation analysis in the (w, δ) plane reveals how the interplay between protection costs and social norms governs long-term lake states. When the protection cost w is low, the system converges to a single stable equilibrium $E_{01} = (0, 1)$, corresponding to universal pro-environmental behavior and a nutrient-poor lake. In contrast, when w is sufficiently high, only the equilibrium $E_{30} = (P_{30}, 0)$ remains stable, representing the collapse of environmental protection and a persistently eutrophic lake state. For weak social norms (δ small), the system admits a unique interior stable equilibrium $E_* = (P_*, x_*)$, where partial environmental engagement leads to an intermediate

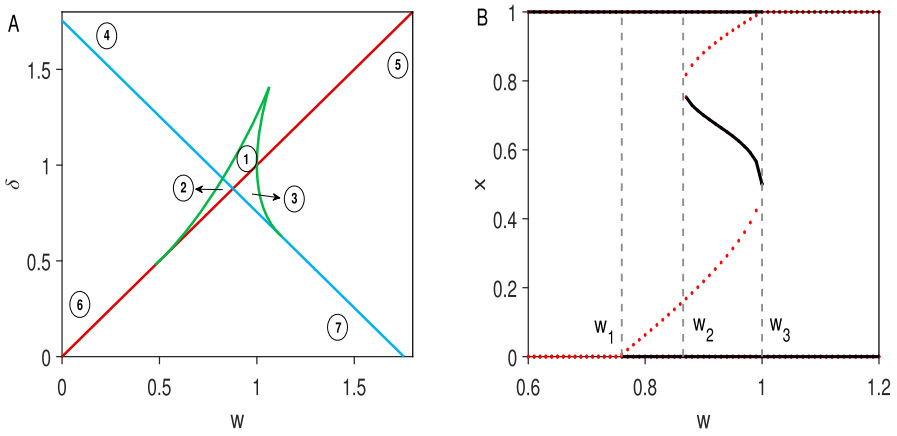

Fig. 4 (**A**) Two-parameter bifurcation diagram for model (5) in the (w, δ) parameter plane. Stability regions include monostability at $E_{01} = (0, 1)$ (region 6), $E_{30} = (P_{30}, 0)$ (region 5), and $E_* = (P_*, x_*)$ (region 7); bistability between E_{01} and E_* (region 2), between E_{30} and E_* (region 3), and between E_{01} and E_{30} (region 4); and tristability between E_{01}, E_*, and E_{30} (region 1). (**B**) One-parameter bifurcation diagram of conservationists (x) with respect to conservation cost (w) for fixed $\delta = 1$. Here $w_1 = 0.76$, $w_2 = 0.86$, $w_3 = 1$. Social learning rate $k = 0.2$ as well as recycling rate of phosphorus $r = 1$ and other parameter values are shown in Table 2

ecological state. As δ increases, stronger social norms polarize individual behavior, giving rise to bistability between oligotrophic (E_{01}) and eutrophic (E_{30}) states. Moreover, intermediate combinations of w and δ generate richer multistability structures: bistability between E_{01} and E_*, or between E_{30} and E_*, and even tristability where E_{01}, E_{30}, and E_* are simultaneously stable. These results demonstrate that moderate protection costs combined with strong social norms can substantially increase sensitivity to initial conditions, highlighting the potential for regime shifts in coupled human-environment models.

Fixing $\delta = 1$, we implement an additional one-parameter bifurcation diagram in Fig. 4 (B) to display that changing the value of w results in various dynamics regimes, including monostability, bistability, and tristability. Specifically,

- When $w \leq w_1 = 0.76$, i.e., for a relatively small value of w, model (5) has a unique equilibrium point E_{01}, defined by full conservationism and no phosphorus (the oligotrophic state), is numerically globally attracting. In this case model (5) is monostable.
- When $w \geq w_3 = 1$, i.e., for a relatively large value of w, model (5) has a unique equilibrium point E_{30}, defined by no conservationists and a relatively high concentration of phosphorus (the eutrophic state), is also globally attracting. Within this parameter interval, model (5) is similarly monostable.
- When $w_1 < w < w_3$, i.e., for an intermediate value of w, model (5) can occur multistable scenario. More precisely,
  - For $w_1 < w \leq w_2$, model (5) has two stable equilibria: E_{01} and E_{30}, which correspond respectively to a full conservationism state and a no conservationists state; and one saddle point E_3. Actually, the emergence of bistability is

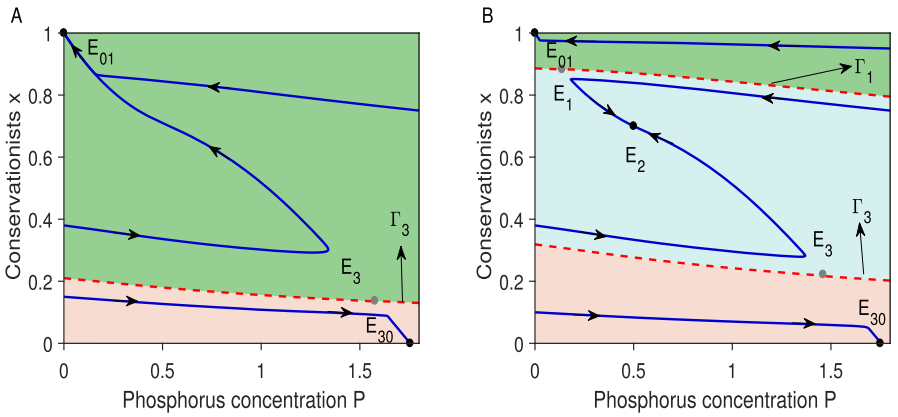

Fig. 5 Phase plane for intermediate values of w. (**A**) $w = 0.85$, taken from interval $[w_1, w_2]$, while (**B**) $w = 0.9$, taken from interval $[w_2, w_3]$. The shaded regions represent the attraction basin of the respective equilibrium. E_1 and E_3 are saddle points, and their stable manifolds (Γ_1 and Γ_3) form the separatrices of the basin of attraction, i.e., the red dashed lines

a common result in mathematical models with replicator dynamics equations simulating human behavior due to the highly nonlinear nature of coupled models.

– As the parameter w increases further until it crosses the critical value w_2, i.e., $w_2 < w < w_3$, an interior equilibrium E_2 emerges through a saddle-node bifurcation, and model (5) undergoes a transition from bistability to tristability.

It is important to emphasize that only multistability between equilibria is shown here; in fact, for a relatively large social learning rate κ, the interior equilibrium will become unstable and branch out into a stable limit cycle through Hopf bifurcation, so model (5) may undergo bistable or tristable between the equilibrium point and the limit cycle. Furthermore, if the P-nullcline is S-shaped, which depends on the nature of the lake and is independent of human behavior, model (5) has up to four equilibria stable simultaneously.

As a typical example of a bistable scenario, we fix $w = 0.85$ and the other parameter values are the same as in Fig. 4 (B), and then the phase portrait of model (5) is shown in Fig. 5 (A). Here, the green and pink regions represent the basins of attraction of equilibria E_{01} and E_{30}, respectively, which are separated by the stable manifold of saddle point E_3 (red dashed line). As one can see, the trajectories with an initial value above Γ_3 tend to E_{01}, and the trajectories with an initial value below Γ_3 approach E_{30}. We now show the dynamics for another intermediate w value ($w = 0.9$) that allows the tristable case to occur. As shown in Fig. 5 (B), when w belongs to the interval $[w_2, w_3]$, in addition to the two extreme equilibria E_{01} and E_{30} being stable, the equilibrium corresponding to the intermediate level of the proportion of conservationists is also stable. The stable manifold of saddle points E_1 and E_3 divides the first quadrant into three regions, which correspond to three different levels of the proportion of conservationists in the population. In this regard, the equilibrium to which the system converges would depend on the initial conditions of the coupled system.

5 Rate-induced tipping in the coupled human-environment model

One potential strategy to prevent the eutrophication of lakes is for governments to implement management policies that include increased fines for non-environmental protectors and incentives for environmental protectors. Additionally, awareness-raising campaigns, such as reinforcing anti-pollution social norms that require significant human and material resources, should also be effectively implemented. While management policies are publicized and implemented, the cost of lake protection, both in terms of time and money, can increase significantly as society develops. Therefore, in addition to the size of lake protection costs, it is necessary to study the effects of the rate of increase in conservation costs on lake nutrient levels and the proportion of people who support environmental protection in the population. In this section, we first give important concepts related to rate-induced tipping and then explore the relationship between lake eutrophication and the rate of growth of conservation costs.

5.1 Basin instability on a parameter path

Roughly speaking, rate-induced tipping occurs when a system deviates too far from its moving equilibrium due to rapid changes in time-varying parameters, and this tipping mechanism usually does not involve any bifurcation. In essence, if the parameters change fast enough, the system cannot keep track of continuously changing attractors. Although the analysis used to investigate bifurcation-induced tipping relies on the parameter w crossing its bifurcation point, rate-induced tipping does not require any special assumptions about the magnitude of w. The crucial notion for understanding R-tipping is basin instability, and before defining it, we require the following elements: (i) Multistability in the autonomous system: for each input parameter, model (5) has at least two stable attractors. For example, the coupled human-environment model exhibits tristability between E_{01}, E_{30} and E_2 in Fig. 5 (B); (ii) A continuous parameter path Δ that does not cross any bifurcation points. For example, the parameter path (w_2, w_3) is between two saddle-node bifurcation points; (iii) The basin of attraction of a stable equilibrium $E(p)$ in the autonomous system for parameter p, defined as the set of initial states (P_0, x_0) whose trajectories converge to $E(p)$:

$$B(E, p) = \left\{(P_0, x_0) \in \mathbb{R}^2 : (P(t), x(t)) \to E(p), t \to +\infty\right\}.$$

In the following, for the case of bistability, we define the basin instability associated with initial states. This definition can be naturally extended for systems with multiple attractors.

Definition 1 Suppose that an autonomous system with a continuous parameter path Δ has two local asymptotically stable equilibria $E_i(p)$, $i = 1, 2$, and their positions vary with the parameter p. Let $\overline{B(E_i, p)}$ denote the basin of attraction of $E_i(p)$ together with its boundary. We say that the initial point (P_0, x_0) is basin unstable on the path Δ if there are two values $p_1, p_2 \in \Delta$, such that the initial state (P_0, x_0) originally

belonged to the basin of attraction $\overline{B(E_2,\, p_1)}$, but now belongs to the basin of attraction $\overline{B(E_1,\, p_2)}$.

The notion of basin instability here is for all initial states of model (5), which extends the ideas in Ref. (O'Keeffe and Wieczorek 2020), where they considered the basin instability of the attractor of the autonomous system. Using this definition, we identify that the region between the boundaries Γ_1 and $\widetilde{\Gamma}_1$ (or between Γ_3 and $\widetilde{\Gamma}_3$) of the attraction domains is basin unstable on the path [0.87, 0.98] (see Fig. 6). We next focus only on these two places with basin instability and do not look at the upper, middle, and lower three white regions as shown in Fig. 6, since the fate of the trajectories from the white areas is independent of the rate of change of w.

5.2 Lake eutrophication due to rate-induced critical transitions

To capture the impact of changes in conservation costs over time, we consider the parameter w in model (5) as a function of time, $w_2 < w(t) < w_3$, where w_2 and w_3 are bifurcation points discussed in subsection 4.2. By holding $w(t)$ between w_1 and w_2, we rule out the possibility of b-tipping as the cost of protection changes and focus instead on the potential for rate dependence in response to changing w. It is important to emphasize that within the range of $w(t)$ we allow here, the model has three steady states corresponding to full conservationism (the oligotrophic state), intermediate levels of conservationism (the intermediate nutritional state), and no conservationism (the eutrophic state).

According to our aim to study rate-induced critical transitions, a continual increase in $w(t)$ can be written as,

$$w(t) = \begin{cases} w_2 + \varepsilon + \lambda t & \text{while } \; w(t) < w_3 - \varepsilon, \\ w_3 - \varepsilon & \text{otherwise,} \end{cases} \tag{6}$$

where λ is the rate of the increase and ε is a small parameter to ensure that w never reaches the bifurcation points at w_2 and w_3. Eq. (6) ensures that the cost of conservation increases linearly to a maximum value of $w_3 - \varepsilon$ and then remains constant. We know from subsection 5.1 that for the parameter path (0.87, 0.98), two regions (the yellow and cyan-shaded regions) are basin unstable; that is, the solution trajectory starting from that region may cause tipping events, which depend on the rate at which the parameter w changes.

Simulating model (5) with a parameter w that varies according to Eq. (6), we find that the most interesting is the possibility of shifting between the steady states as the cost of conservation, w, changes over time. Fig. 6 shows the phase portrait of the system (5) with linearly increasing conservation cost w at different rates of change λ. In Fig. 6 (A), the trajectory from the cyan-shaded area converges to an intermediate nutrient level state ($\widetilde{E}_2$) for a smaller rate of change ($\lambda = 0.001$); however, for a larger rate of change ($\lambda = 0.01$), it eventually converges to a eutrophic state (E_{30}). Similarly, as shown in Fig. 6 (B), the trajectory from the yellow-shaded area converges to an oligotrophic state (E_{01}) for a smaller rate of change ($\lambda = 0.0004$); however, for a larger

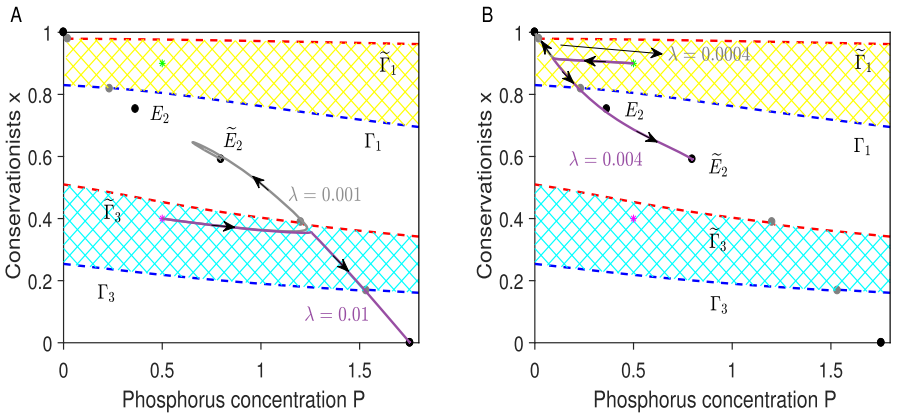

Fig. 6 Phase portrait of the system (5) with linearly increasing conservation cost w at different rates of change. (**A**) The trajectory from the cyan-shaded area converges to an intermediate nutrient level state ($\widetilde{E}_2$) for a smaller rate of change ($\lambda = 0.001$); however, for a larger rate of change ($\lambda = 0.01$), it eventually converges to a eutrophic state (E_{30}). (**B**) Similarly, the trajectory from the yellow-shaded area converges to an oligotrophic state (E_{01}) for a smaller rate of change ($\lambda = 0.0004$); however, for a larger rate of change ($\lambda = 0.004$), it eventually converges to an intermediate nutritional state ($\widetilde{E}_2$). The initial states in the yellow and cyan-shaded regions are basin unstable. Γ_1 and Γ_3 are the attraction domain boundaries corresponding to $w = 0.87$, while $\widetilde{\Gamma}_1$ and $\widetilde{\Gamma}_3$ are the attraction domain boundaries corresponding to $w = 0.98$. E_2 and $\widetilde{E}_2$ are the internal steady states at $w = 0.87$ and 0.98, respectively. Green and magenta asterisks mark the locations of the initial points (0.5, 0.9) and (0.5, 0.4), respectively

rate of change ($\lambda = 0.004$), it eventually converges to an intermediate nutritional state ($\widetilde{E}_2$). These results suggest that too rapid an increase in the cost of conservation can shift a lake from an intermediate to a eutrophic state or from an oligotrophic state to an intermediate state, which is related to the choice of initial state. In short, R-tipping always undermines management objectives in these cases and is therefore a phenomenon to be avoided rather than a management tool to be utilized.

5.3 The effect of the rate of change of *w* on the basin of attraction

By subsection 5.2, trajectories starting from places with basin instability converge to different attractors depending on the magnitude of the λ, as exemplified in Fig. 6. Therefore, it is necessary to reconstruct the basin of attraction when considering the cost of conservation as a time-varying parameter. Note that the upper, middle, and lower white regions always belong to the basin of attraction of the E_{01}, E_2, and E_{30} attractors, respectively, independent of the size of the λ.

The process of changing the basins of attraction for oligotrophic (E_{01}), intermediate (E_2), and eutrophic (E_{30}) states at $\lambda = 0$, 0.001, and 0.01 is illustrated in Fig. 7. Here, the blue, green, and red shaded areas correspond to the attraction domains of the oligotrophic, intermediate, and eutrophic states, respectively. As shown in Fig. 7 (A), when the rate of change is zero, i.e., the cost of conservation remains constant, the basin of attraction of each attractor is the same as when the autonomous system (5) has parameter $w = 0.87$. The trajectory from the region above Γ_1 tends to E_{01}; the

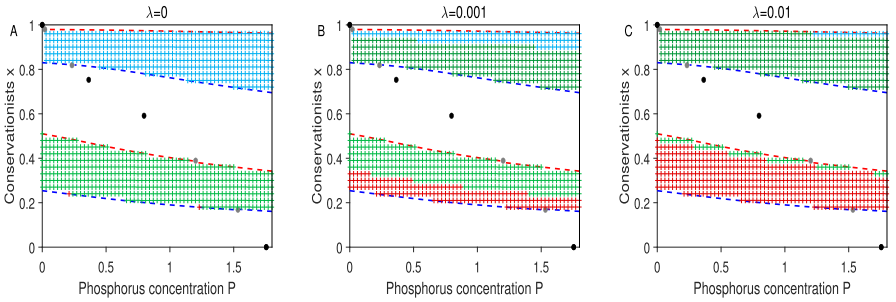

Fig. 7 Reconstruction of the basin of attraction for three different rates of parameter change. The blue, green, and red shaded areas correspond to the attraction domains of the oligotrophic (E_{01}), intermediate (E_2), and eutrophic (E_{30}) states, respectively. The upper, middle, and lower white regions always belong to the basin of attraction of the E_{01}, E_2, and E_{30} attractors, respectively, independent of the size of the λ

trajectory from the region between Γ_1 and Γ_3 tends to E_2; however, the trajectory from below Γ_3 ends up at E_{30}. As λ increases to 0.001, red shading appears between Γ_3 and $\widetilde{\Gamma}_3$, i.e., trajectories from this region that would have converged to an intermediate state are forcing the system to converge to an eutrophic state in the face of rapidly increasing conservation costs (see Fig. 7 (B)). When the rate of change λ is relatively large, the blue shaded region disappears completely. It is gradually replaced by green shading, suggesting that only the tiny region above the red dashed line ($\widetilde{\Gamma}_1$) in the first quadrant is safe. In contrast, trajectories departing from the area below $\widetilde{\Gamma}_1$ converge to an intermediate or eutrophic state (see Fig. 7 (C)).

To show the relationship between the relative areas of the attraction domains corresponding to the three different trophic states and the rate of change λ, we calculate the proportion of the total area occupied by each attraction domain for different λ. In Fig. 8 (A), for each λ, the blue, green, and red dotted lines indicate the percentage of the basin of attraction occupied by the oligotrophic, intermediate, and eutrophic attractors, respectively. Obviously, as the rate of change in the cost of conservation increases, the basin of attraction corresponding to the oligotrophic attractor first gradually decreases and then reaches a stationary value, while the basin of attraction corresponding to the eutrophic state gradually expands. Interestingly, unlike the previous two scenarios, the size of the basin of attraction for the intermediate state attractor shows a non-monotonic trend, i.e., it first increases and then decreases, reaching a maximum at $\lambda = 0.001$. This suggests that there exists a suitable threshold λ to maximize the basin of attraction for the intermediate trophic level. In addition, we find that once the cost of conservation begins to increase linearly, even if the rate of increase is slow, e.g., $\lambda = 0.001$, the dangerous area (red and green curves) increases significantly, while the safe zone (blue curve) decreases dramatically.

5.4 R-tipping probability

In this subsection, we first give an essential concept: *rate-tipping probability*. We then investigate how the rate of change of the conservation cost λ affects the rate-tipping probability. Based on the definition 2, instead of studying the critical rate for each

initial condition, we will investigate the R-tipping probability of a large set of initial conditions obtained from the relevant regions with basin instability.

Definition 2 We call the probability that the trajectory starting from the cyan-shaded (or yellow-shaded) region crosses the boundary Γ_3 (or Γ_1) and settles within the basin of attraction of steady state E_{30} (or $\widetilde{E}_2$) as the rate-tipping probability.

Below, we provide the detailed procedure for calculating the rate-tipping probability. To calculate the probability of rate-induced tipping from the intermediate nutritional state ($\widetilde{E}_2$) to the eutrophic state (E_{30}), we solve model (5) with time-varying parameter $w(t)$ for a large number of initial conditions chosen from the (P, x) phase space and record the final state of the trajectory. For each fixed rate λ, if the final state is still in an intermediate nutritional state, then no R-tipping occurs for the particular initial condition. Otherwise, if the final state is the eutrophic state, then R-tipping occurs for this λ. Numerically, the tipping probability can be approximated by the fraction of the number of initial conditions leading to R-tipping out of the whole chosen initial conditions,

$$\mathbb{P}_{eutrophic} = \frac{n}{N},$$

where N denotes the total number of selected initial points from the first quadrant and n denotes the number of trajectories ending in eutrophication. For calculating the value of N, we partition the region $[0, 1.8] \times [0, 1]$ into 61×34 subintervals with a granularity of 0.03, hence $N = 2074$. For determining the value of n, we iteratively traverse all initial points and simulate model (5) with time-varying parameter $w(t)$ using the *ode45* function in Matlab for each fixed λ. In this step, the simulation time is set long enough to eliminate transient solutions. Similarly, we can calculate the probability of rate-induced tipping from the oligotrophic state (E_{01}) to the intermediate nutritional state ($\widetilde{E}_2$).

Fig. 8 (B) shows the relationship between the rate-induced tipping probability and λ. Here the red dotted line indicates the probability of tipping from an intermediate trophic state ($\widetilde{E}_2$) to a eutrophic state (E_{30}), while the green dotted line indicates the probability of tipping from an oligotrophic state (E_{01}) to an intermediate trophic state ($\widetilde{E}_2$). We find that as λ increases, the tipping probability first increases rapidly, then slowly, and finally saturates. Interestingly, the R-tipping probability increases rapidly when λ is slightly greater than zero, which is consistent with the findings in subsection 5.3. This implies that once the cost of conservation begins to increase, the probability of eutrophication in lakes also rises significantly. Lake managers must come up with effective measures in time to deal with this bad situation. Furthermore, as λ becomes larger, the probability of tipping from an oligotrophic state to an intermediate nutrient state is always greater than switching from an intermediate nutrient state to eutrophication. When λ is at the middle level, i.e., $\lambda = 0.01$, the tipping probabilities are equal. However, when λ is large enough, i.e., $\lambda > 0.01$, the probability of rate-induced tipping from $\widetilde{E}_2$ to E_{30} prevails. This suggests that the rapid increase in conservation costs promotes the eutrophication of the lake.

In Fig. 9, we also present the dependence of the R-tipping probability on the parameter change rate λ for different levels of injunctive social norms intensity δ and social learning rate κ. Our results highlight the critical role of social processes in shaping the

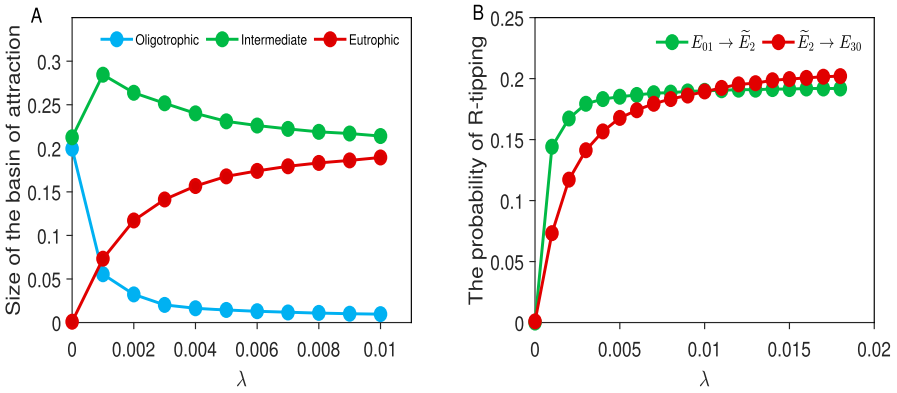

Fig. 8 (**A**) The relationship between the area percentage of the attraction domain corresponding to the three different nutrient states and the rate of change of the parameter. The blue, green, and red dotted lines indicate the percentage of the basin of attraction occupied by the oligotrophic, intermediate, and eutrophic attractors, respectively. (**B**) The relationship between the probability of rate-induced tipping and λ. The red dotted line indicates the probability of tipping from an intermediate trophic state ($\widetilde{E}_2$) to a eutrophic state (E_{30}), while the green dotted line indicates the probability of tipping from an oligotrophic state (E_{01}) to an intermediate trophic state ($\widetilde{E}_2$)

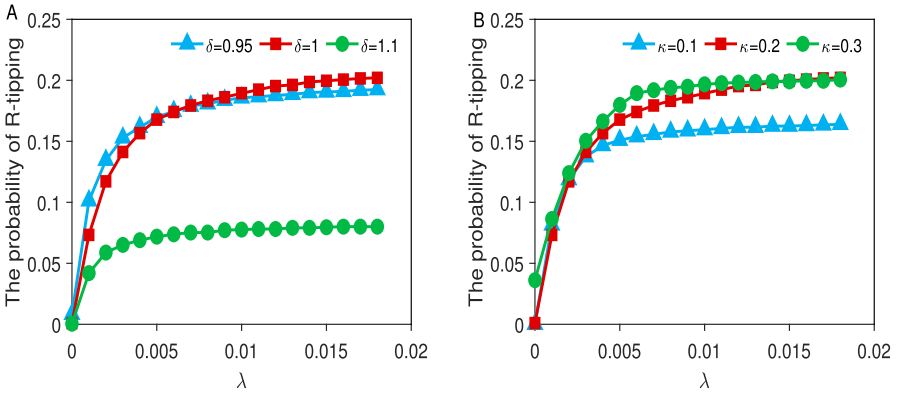

Fig. 9 The relationship between the probability of tipping from $\widetilde{E}_2$ to E_{30} and the parameter change rate λ for different δ and κ

resilience of coupled social-ecological lake systems. As the rate of parameter change λ increases, i.e., representing a faster rise in environmental protection costs, the probability of R-tipping consistently increases, because the social subsystem cannot adjust fast enough to counteract rapid environmental degradation. The strength of social norms δ substantially modulates this risk: a sufficiently large δ (e.g., $\delta = 1.1$) sustains a high level of pro-environmental behavior even under rapidly shifting conditions, thereby reducing the likelihood of R-tipping. In contrast, when δ is small, the collective response remains weak, and the system remains highly vulnerable to a regime shift even when external changes occur slowly. In opposition to δ, the social learning rate κ has an opposite effect on system resilience. Smaller values of κ dampen rapid behavioral switching and reduce the chance that transient social fluctuations trigger

a collapse in cooperation, leading to lower R-tipping probabilities. As κ increases, however, individuals adjust their behavior more rapidly in response to environmental and social cues, amplifying short-term feedbacks and making the system more prone to crossing critical thresholds under the same rate of environmental change. Together, these findings indicate that strong social norms enhance resilience to fast-moving environmental deterioration, whereas overly rapid social learning can destabilize collective environmental action, underscoring the dual and contrasting roles of social norm strength and learning speed in governing regime shift risk in social-ecological systems.

6 Discussion

The majority of natural ecosystems are heavily impacted by anthropogenic activities. At the same time, alterations in ecosystems in turn affect human behavioral decisions, thus forming a feedback cycle. Mathematically, models depicting such feedback loops are called human-environment coupled systems, and other terms such as “socio-ecological systems" and “human-nature coupled systems" are also employed to characterize such phenomena (Berkes et al. 2000). This class of nonlinear systems can usually undergo regime shifts from one stable attractor to another (Farahbakhsh et al. 2024). In addition to perturbations from random noise and the crossing of a particular critical threshold by external conditions that can lead to regime shifts, the rapid rate of change in environmental pressures has also been identified as an essential potential contributor to such critical transitions (Ritchie et al. 2023). However, the effect of the change rate of model parameters on the critical transition in coupled human-environment systems has not been fully evaluated.

In this paper, we use the replicator equation to describe the human behavioral decision-making process and couple it with the phosphorus dynamics model proposed by Carpenter et al. (Carpenter et al. 1999). The coupled model has two sources of nonlinearity: the first is in the social subsystem, where attitudes toward environmental protection in the population tend to two extremes due to a high degree of herd mentality; the second is in the ecological subsystem, where nutrient levels tend to bistability due to the rapid recycling of phosphorus in the lake. When the two subsystems are entangled, the coupled model exhibits multiple steady states and periodic oscillatory regimes. Analysis of the model reveals that the stability of the desirable state (0, 1), i.e., the state of no anthropogenic phosphorus loading and complete conservationism, depends on the cost of conservation and the strength of social norms. Specifically, weak social norms and a high cost of conservation can destabilize equilibrium (0, 1). However, a smaller social learning rate strengthens the stability of the intermediate state E_2, i.e., the partial conservationist. We also use the cost of conservation as a bifurcation parameter to find that model (5) appears to have a variety of dynamics regimes, including mono-stable, bi-stable, and tri-stable. These theoretical results suggest that complex dynamical behavior may occur in coupled models compared to uncoupled models.

We are mainly concerned with the tri-stability scenario when there are three steady states in model (5): oligotrophic, intermediate, and eutrophic. The most interesting

is the possibility of shifting between the steady states as the cost of conservation, w, changes over time. Concretely, we identify that the region between the boundaries Γ_1 and $\widetilde{\Gamma}_1$ (or between Γ_3 and $\widetilde{\Gamma}_3$) of the attraction domains is basin unstable on a specified parameter path (see Fig. 6). Basin instability and critical rates are prerequisites for the occurrence of rate-induced tipping. For example, as long as w increases slowly enough (small λ), the trajectory from the cyan-shaded area (between Γ_3 and $\widetilde{\Gamma}_3$) tends to an intermediate state. Conversely, increasing the cost of conservation too quickly (large λ) can cause R-tipping and move the system into an eutrophic state (see Fig. 6 (A)). In another case, for a trajectory departing from the yellow-shaded region (between Γ_1 and $\widetilde{\Gamma}_1$), there also exists a critical rate beyond which the system undergoes R-tipping and is attracted to the intermediate trophic state (see Fig. 6 (B)). In summary, rapidly increasing conservation costs are detrimental to lake conservation, which may push the model either into an attraction domain with moderate levels of nutrition and a moderate percentage of conservationists or into an attraction domain with eutrophication and a zero percentage of conservationists.

We also explore how the rate of increase in conservation costs affects the size of basins of attraction for three steady states, as shown in Fig. 8 (A). The results show that as the change rate of w increases, the basin of attraction corresponding to the oligotrophic attractor first gradually decreases and then reaches a stationary value, while the basin of attraction corresponding to the eutrophic state gradually expands. However, for the intermediate state, the size of its basin of attraction shows a non-monotonic trend of increasing and then decreasing. In addition, the relationship between the size of the attraction domain and the rate of change λ shows that the size of the basin of attraction of oligotrophic decreases significantly as long as λ increases a little from 0.

To evaluate rate-tipping risk, we introduce the notion of rate-tipping probability and give a detailed numerical calculation process. As shown in Fig. 8 (B), we find that as λ increases, the tipping probability from E_{01} to $\widetilde{E}_2$ (or from $\widetilde{E}_2$ to E_{30}) first increases rapidly, then slowly, and finally saturates. Interestingly, the rate of change λ has a threshold below which the probability of tipping from an oligotrophic state (E_{01}) to an intermediate nutrient state ($\widetilde{E}_2$) is always greater than switching from an intermediate nutrient state to a eutrophic state. Above this threshold, however, the probability of rate-induced tipping from $\widetilde{E}_2$ to E_{30} prevails. This suggests that the rapid increase in conservation costs promotes the eutrophication of the lake. Meanwhile, this gives lake managers the insight that limiting only the magnitude of lake conservation costs is not sufficient to control lake deterioration and that the rate of increase in conservation costs should also be considered.

Our results suggest that rapid increases in protection costs or environmental pressures can induce regime shifts even when classical static thresholds are not crossed. Strong social norms substantially reduce this risk by maintaining collective environmental action, whereas weak norms leave systems vulnerable even under slowly changing conditions. Together, these findings highlight the importance of strengthening social institutions and anticipating the pace of environmental change when designing lake management strategies.

Although we only studied a two-dimensional model in this work, it is necessary to emphasize that the methods in this paper are applicable to any ecosystem

model with multiple alternative steady states. In the future, we will examine how human pollution discharge impacts phytoplankton blooms within a higher-dimensional human-environment coupling model. In addition, for systems with alternative stable states, environmental noise can have a significant effect on their dynamics, which may cause stochastic trajectories to switch frequently between multiple attractors, also known as N-tipping, as mentioned in the introduction. An interesting direction for future research is to investigate whether N-tipping due to random variability and R-tipping due to parameter shifts are independent of each other, and if not, how these different mechanisms interact to induce eutrophication in lakes.

Appendix A Proof of Theorem 1

Proof It is obvious that model (5) always has a boundary equilibrium $E_{01} = (0, 1)$. When the population is in full protectionism, that is $x = 1$, the boundary equilibrium $(P, 1)$ should satisfy $hP^2 - rP + hm^2 = 0$. It is easy to verify that if $r > 2hm$, this equation has two positive real roots $P_{11} = \frac{r-\sqrt{r^2-4h^2m^2}}{2h}$ and $P_{21} = \frac{r+\sqrt{r^2-4h^2m^2}}{2h}$, which means model (5) have two boundary equilibria. In the following, we focus on the stability of these boundary equilibria.

(1) Stability of equilibrium E_{01}. Since the Jacobian matrix of model (5) evaluated at $E_{01} = (0, 1)$ is given by

$$J(E_{01}) = \begin{pmatrix} -h & -\alpha \\ 0 & \kappa(w-\delta) \end{pmatrix},$$

it follows that $\lambda_1 = -h$ and $\lambda_2 = \kappa(w - \delta)$. That is, the equilibrium E_{01} is locally stable if $w < \delta$; while if $w > \delta$, E_{01} is unstable.

(2) Stability of equilibrium E_{11}. The Jacobian matrix at E_{11} can be shown as

$$J(E_{11}) = \begin{pmatrix} \frac{2rm^2P_{11}}{(m^2+P_{11}^2)^2} - h & -\alpha \\ 0 & \kappa(w-\delta-P_{11}) \end{pmatrix}.$$

We have $\lambda_1 = -\frac{2h(r(r^2-4h^2m^2)-\sqrt{r^2-4h^2m^2}(r^2-2h^2m^2))}{r(\sqrt{r^2-4m^2h^2}-r)^2} > 0$. Therefore, E_{11} is a saddle whenever it exists.

(3) Stability of equilibrium E_{21}. Evaluating the Jacobian matrix at E_{21}, we have

$$J(E_{21}) = \begin{pmatrix} \frac{2rm^2P_{21}}{(m^2+P_{21}^2)^2} - h & -\alpha \\ 0 & \kappa(w-\delta-P_{21}) \end{pmatrix}.$$

The corresponding eigenvalues are given by $\lambda_1 = \frac{2h(r(4h^2m^2-r^2)+\sqrt{r^2-4h^2m^2}(2h^2m^2-r^2))}{r(\sqrt{r^2-4m^2h^2}+r)^2}$ < 0, and $\lambda_2 = \kappa(w - \delta - P_{21})$. Therefore, equilibrium E_{21} is locally stable if $w < \delta$; while if $w - \delta > P_{21}$, equilibrium E_{21} is unstable.

Following the Jacobian matrix, if $r = 2hm$, the characteristic equation at $E_{31} = (\frac{r}{2h}, 1)$ has a zero characteristic root, which indicates that E_{31} is a degenerate equilibrium. Now we determine the type of E_{31} for $r = 2hm$. To this end, we translate E_{31} to the origin by letting $u = P - \frac{r}{2h}$ and $v = x - 1$, then model (5) becomes as

$$\begin{aligned} \frac{\mathrm{d}u}{\mathrm{d}t} &= a_{01}v + a_{20}u^2 + O(|u, v|^3), \\ \frac{\mathrm{d}v}{\mathrm{d}t} &= b_{01}v + b_{11}uv + b_{02}v^2 + O(|u, v|^3), \end{aligned} \tag{7}$$

where $a_{01} = -\alpha$, $a_{20} = \frac{16rm^2h^4(4h^2m^2-3r^2)}{(4h^2m^2+r^2)^3}$, $b_{01} = \frac{\kappa(2hw-2\delta h-r)}{2h}$, $b_{11} = -\kappa$, $b_{02} = \frac{\kappa(2hw-6\delta h-r)}{2h}$. Further making transformation $U = -\frac{1}{a_{01}}u + \frac{1}{b_{01}}v$, $V = \frac{1}{b_{01}}v$ on system (7), we obtain

$$\begin{aligned} \frac{\mathrm{d}U}{\mathrm{d}t} &= l_1U^2 + l_2UV + l_3V^2 + O(|U, V|^3), \\ \frac{\mathrm{d}V}{\mathrm{d}t} &= b_{01}V + O(|U, V|^2), \end{aligned} \tag{8}$$

where $l_1 = -\frac{\alpha h}{2m}$, $b_{01} = \kappa(w - \delta - m)$. Obviously, l_1 determines the codimension of the saddle-node bifurcation if $b_{01} \neq 0$. Therefore, if $w \neq \delta + m$, E_{31} is a saddle-node of codimension 1 according to Theorems $7.1 - 7.3$ in Zhang (1992). This completes the proof of Theorem (1). □

Appendix B Proof of Theorem 2

Proof When the conservationists in the population are absent, that is $x = 0$, model (5) reduces to the ecological subsystem (1). The P component of the boundary equilibrium $(P, 0)$ should satisfy $\alpha + \frac{rP^2}{m^2+P^2} - hP = 0$. We rewrite the above equation as

$$hP - \alpha = \frac{rP^2}{m^2 + P^2}. \tag{9}$$

Let $y_1(P) = hP - \alpha$, and $y_2(P) = \frac{rP^2}{m^2+P^2}$. Notice that $y_1(P)$ and $y_2(P)$ have the following properties: (1) $y_1(0) = -\alpha$, $y_1(+\infty) = +\infty$, $y_2(0) = 0$, $y_2(+\infty) = r$; (2) $y_2(P)$ is increasing in $(0, +\infty)$ with inflexion point P_0 and it is concave in $[0, P_0]$ and convex in $[P_0, +\infty)$, where $P_0 = \frac{\sqrt{3}m}{3}$. The point of tangency between the straight line y_1 and the curve y_2 is the key to determining the number of points where the two curves intersect. The tangency occurs if Eq. (9) is satisfied and also

$$h = \frac{2rm^2P}{(m^2 + P^2)^2} := \beta(P). \tag{10}$$

Substituting Eq. (10) into (9) yields $(r+\alpha)P^4 + m^2(2\alpha - r)P^2 + \alpha m^4 = 0$. It is easy to verify this equation has two roots $P_- = \sqrt{\frac{m^2(r-2\alpha-\sqrt{r^2-8r\alpha})}{2(r+\alpha)}}$ and $P_+ = \sqrt{\frac{m^2(r-2\alpha+\sqrt{r^2-8r\alpha})}{2(r+\alpha)}}$ for $r > 8\alpha$. Consequently, model (5) has three boundary equilibria for $\beta(P_-) < h < \beta(P_+)$, two boundary equilibria for $h = \beta(P_-)$ or $h = \beta(P_+)$, and a unique boundary equilibrium for $h < \beta(P_-)$ or $h > \beta(P_+)$.

In the following, we investigate the stability of these boundary equilibria $E_{i0} = (P_{i0}, 0)$, $i = 1, 2, 3$ when it exists. The Jacobian matrix of model (5) evaluated at $E_{i0} = (P_{i0}, 0)$, $i = 1, 2, 3$ is

$$J(E_{i0}) = \begin{pmatrix} \frac{2rm^2 P_{i0}}{(m^2+P_{i0}^2)^2} - h & -\alpha \\ 0 & \kappa(P_{i0} - w - \delta) \end{pmatrix}.$$

The corresponding eigenvalues are given by $\lambda_1 = \frac{2rm^2 P_{i0}}{(m^2+P_{i0}^2)^2} - h$, $\lambda_2 = \kappa(P_{i0} - w - \delta)$. Therefore, if $x = 0$, any boundary equilibrium with $P_{i0} > w + \delta$, $i = 1, 2, 3$, must be unstable. However, for a boundary equilibrium with $P_{i0} < w + \delta$, $i = 1, 2, 3$, the sign of λ_1 is determined by the slope difference of the two curves $y_1(P)$ and $y_2(P)$ at the intersection, which determines the stability of the equilibrium. Thus, when the model has three boundary equilibria, the equilibrium state with an intermediate P-coordinate (i.e., P_{20}) is a saddle point, while both E_{10} and E_{30} are locally asymptotically stable. This completes the proof of Theorem (2). □

Appendix C Proof of Theorem 3

Proof According to the right-hand side function of model (5), the interior equilibria $E = (P, x)$ is the intersection of two curves $f_1(P) = \alpha + \frac{rP^2}{m^2+P^2} - hP$ and $f_2(P) = \frac{\alpha}{2\delta}(-P + w + \delta)$, where P coordinate satisfies

$$F(P) = (\alpha - 2\delta h)P^3 + (2\delta r + \alpha\delta - \alpha w)P^2 + m^2(\alpha - 2\delta h)P + \alpha m^2(\delta - w) = 0. \quad (11)$$

The cubic equation (11) has at most three positive roots. Note that when $\delta = w$, equation (11) has a solution $P = 0$ associated with the equilibrium of full conservationism and no phosphorus emissions (0, 1). To decide the number of positive roots of $F(P)$, we calculate Δ_0 the discriminant of $F(P)$ with respect to P. Then we have

$$\Delta_0 = \Delta_0(m) = 12m^2\left[a_2(\delta)m^4 + a_1(\delta)m^2 + a_0(\delta)\right],$$

and

$$a_2(\delta) = (\alpha - 2\delta h)^4, a_1(\delta) = (\alpha - 2\delta h)^2\left[2(w-\delta)^2\alpha^2 + 10r\delta(w-\delta)\alpha - r^2\delta^2\right],$$
$$a_0(\delta) = (\delta - w)\left[(\delta - w)\alpha + 2\delta r\right]^3\alpha.$$

We define an auxiliary function $g(m) = a_2(\delta)m^4 + a_1(\delta)m^2 + a_0(\delta)$.

In order to study the roots of Eq. (11), it is necessary to study the roots of function $g(m)$. Let $\Delta_1(\delta)$ be the discriminant of $g(m)$ with respect m^2, and a straightforward calculation leads that $\Delta_1(\delta) = \delta r(2h\delta - \alpha)^4 [(r - 4\alpha)\delta + 4\alpha w]^3$. If we denote the unique positive root of $\Delta_1(\delta) = 0$ as $\delta^* = \frac{4\alpha w}{4\alpha - r}$, then, when $w < \delta < \delta^*$, $\Delta_0(m) = 0$ have two potential positive roots $m = m^-(\delta) = \sqrt{\frac{-a_1(\delta) - \sqrt{\Delta_1(\delta)}}{2a_2(\delta)}}$ and $m = m^+(\delta) = \sqrt{\frac{-a_1(\delta) + \sqrt{\Delta_1(\delta)}}{2a_2(\delta)}}$. Substituting δ^* into $\Delta_0(m) = 0$, we obtain $m^* = \frac{3\sqrt{3}rw}{8hw - 4\alpha + r}$.

In the following, we focus on the stability of interior equilibria. The Jacobian matrix of model (5) at any interior equilibrium $E_* = (P_*, x_*)$ has the form

$$J(E_*) = \begin{pmatrix} \frac{2rm^2 P_*}{(m^2 + P_*^2)^2} - h & -\alpha \\ \kappa x_*(1 - x_*) & 2\kappa\delta x_*(1 - x_*) \end{pmatrix}.$$

Then the corresponding characteristic equation is $\lambda^2 - T(J(E_*))\lambda + D(J(E_*)) = 0$. If λ_1 and λ_2 are the two eigenvalues, then we have the trace $T(J(E_*)) = \lambda_1 + \lambda_2 = f_1'(P_*) + 2\kappa\delta x_*(1 - x_*)$ and determinant $D(J(E_*)) = \lambda_1\lambda_2 = 2\kappa\delta x_*(1 - x_*)[f_1'(P_*) - f_2'(P_*)]$, where $f_1'(P_*) = \frac{2rm^2 P_*}{(m^2 + P_*^2)^2} - h$, $f_2'(P_*) = -\frac{\alpha}{2\delta}$. For any E_*, sign of the $D(J(E_*))$ is determined by the slope difference of the two curves $f_1(P)$ and $f_2(P)$ at the intersection. If we denote $K_i = f_i'(P_*)(i = 1, 2)$ and $\overline{K} = 2\kappa\delta x_*(1 - x_*)$, then when $K_1 < K_2$, $D(J(E_*)) < 0$, the interior equilibrium point is a saddle. If $K_1 > K_2$, then $D(J(E_*)) > 0$, and the real part of the eigenvalues will be both positive or negative depending on the sign of $T(J(E_*))$. The proof is thus completed.

Summarizing the discussions above, we obtain Theorem 3. □

Author Contributions All authors contributed equally in designing and conducting the study.

Funding This work is partially funded by the National Natural Science Foundation of China (No. 12471465 and 12071293) and the Natural Science Foundation of Shanghai (No. 23ZR1445100).

Data Availibility Data sharing not applicable to this article as no datasets were generated or analysed during the current study.

Declarations

Conflict of interest The authors declare that they have no conflict of interest.

Ethical statement The authors declare that the research presented in this manuscript is original and has not been published elsewhere and is not under consideration by another journal. The study was conducted in accordance with ethical principles and guidelines.

References

Ashwin P, Perryman C, Wieczorek S (2017) Parameter shifts for nonautonomous systems in low dimension: bifurcation-and rate-induced tipping. Nonlinearity 30(6):2185. https://doi.org/10.1088/1361-6544/aa675b

Bauch CT (2005) Imitation dynamics predict vaccinating behaviour. P Roy Soc B-Biol Sci 272(1573):1669–1675. https://doi.org/10.1098/rspb.2005.3153
Bauch CT, Sigdel R, Pharaon J et al (2016) Early warning signals of regime shifts in coupled human-environment systems. P Natl Acad Sci USA 113(51):14560–14567. https://doi.org/10.1073/pnas.1604978113
Bennett EM, Reed-Andersen T, Houser JN et al (1999) A phosphorus budget for the lake mendota watershed. Ecosystems 2:69–75. https://doi.org/10.1007/s100219900059
Berkes F, Folke C, Colding J (2000) Linking social and ecological systems: management practices and social mechanisms for building resilience. Cambridge University Press
Binford MW, Brenner M, Whitmore TJ et al (1987) Ecosystems, paleoecology and human disturbance in subtropical and tropical america. Quaternary Sci Rev 6(2):115–128. https://doi.org/10.1016/0277-3791(87)90029-1
Boettiger C (2018) From noise to knowledge: how randomness generates novel phenomena and reveals information. Ecol Lett 21(8):1255–1267. https://doi.org/10.1111/ele.13085
Bury TM, Bauch CT, Anand M (2019) Charting pathways to climate change mitigation in a coupled socio-climate model. PLoS Comput Biol 15(6):e1007000. https://doi.org/10.1371/journal.pcbi.1007000
Carpenter SR, Ludwig D, Brock WA (1999) Management of eutrophication for lakes subject to potentially irreversible change. Ecol Appl 9(3):751–771. https://doi.org/10.2307/2641327
Carpenter SR, Brock WA, Hansen GJ et al (2017) Defining a safe operating space for inland recreational fisheries. Fish Fish 18(6):1150–1160. https://doi.org/10.1111/faf.12230
Dai L, Vorselen D, Korolev KS et al (2012) Generic indicators for loss of resilience before a tipping point leading to population collapse. Science 336(6085):1175–1177. https://doi.org/10.1126/science.1219805
Dodds WK, Bouska WW, Eitzmann JL et al (2009). Eutrophication of us freshwaters analysis of potential economic damages. https://doi.org/10.1021/es801217q
Dokulil MT (2014) Environmental impacts of tourism on lakes. Eutrophication: causes, consequences and control pp 81–88. https://doi.org/10.1007/978-94-007-7814-6_7
Drazin PG (1992) Nonlinear systems. 10, Cambridge University Press
Farahbakhsh I, Bauch CT, Anand M (2022) Modelling coupled human-environment complexity for the future of the biosphere: strengths, gaps and promising directions. Philos T R Soc B 377(1857):20210382. https://doi.org/10.1098/rstb.2021.0382
Farahbakhsh I, Bauch CT, Anand M (2024) Tipping points in coupled human-environment system models: a review. Earth Syst Dynam 15(4):947–967. https://doi.org/10.5194/esd-15-947-2024
Fishburn PC (1970) Utility theory for decision making. Tech. rep, Research analysis corp McLean VA
Galvani AP, Bauch CT, Anand M et al (2016) Human-environment interactions in population and ecosystem health. P Natl Acad Sci USA 113(51):14502–14506. https://doi.org/10.1073/pnas.1618138113
Genkai-Kato M, Vadeboncoeur Y, Liboriussen L et al (2012) Benthic-planktonic coupling, regime shifts, and whole-lake primary production in shallow lakes. Ecology 93(3):619–631. https://doi.org/10.1890/10-2126.1
Gil MA, Baskett ML, Munch SB et al (2020) Fast behavioral feedbacks make ecosystems sensitive to pace and not just magnitude of anthropogenic environmental change. P Natl Acad Sci USA 117(41):25580–25589. https://doi.org/10.1073/pnas.2003301117
Hall RI, Leavitt PR, Quinlan R et al (1999) Effects of agriculture, urbanization, and climate on water quality in the northern great plains. Limnol Oceanogr 44(3part2):739–756. https://doi.org/10.4319/lo.1999.44.3_part_2.0739
Heggerud CM, Wang H, Lewis MA (2022) Coupling the socio-economic and ecological dynamics of cyanobacteria: Single lake and network dynamics. Ecol Econ 194:107324. https://doi.org/10.1016/j.ecolecon.2021.107324
Henderson KA, Bauch CT, Anand M (2016) Alternative stable states and the sustainability of forests, grasslands, and agriculture. P Natl Acad Sci USA 113(51):14552–14559. https://doi.org/10.1073/pnas.1604987113
Ho JC, Michalak AM, Pahlevan N (2019) Widespread global increase in intense lake phytoplankton blooms since the 1980s. Nature 574(7780):667–670. https://doi.org/10.1038/s41586-019-1648-7
Hofbauer J, Sigmund K (2003) Evolutionary game dynamics. B Am Math Soc 40(4):479–519. https://doi.org/10.1090/S0273-0979-03-00988-1
Hopkins E (1999) A note on best response dynamics. Games Econom Behav 29(1–2):138–150

Iwasa Y, Uchida T, Yokomizo H (2007) Nonlinear behavior of the socio-economic dynamics for lake eutrophication control. Ecol Econ 63(1):219–229. https://doi.org/10.1016/j.ecolecon.2006.11.003
Iwasa Y, Suzuki-Ohno Y, Yokomizo H (2010) Paradox of nutrient removal in coupled socioeconomic and ecological dynamics for lake water pollution. Theor Ecol 3:113–122. https://doi.org/10.1007/s12080-009-0061-5
Kiers C, Jones CK (2020) On conditions for rate-induced tipping in multi-dimensional dynamical systems. J Dyn Differ Equ 32:483–503. https://doi.org/10.1007/s10884-019-09730-9
Kuehn C (2013) A mathematical framework for critical transitions: normal forms, variance and applications. J Nonlinear Sci 23:457–510. https://doi.org/10.1007/s00332-012-9158-x
Lade SJ, Tavoni A, Levin SA et al (2013) Regime shifts in a social-ecological system. Theor Ecol 6:359–372. https://doi.org/10.1007/s12080-013-0187-3
Liu J, Dietz T, Carpenter SR et al (2007) Complexity of coupled human and natural systems. Science 317(5844):1513–1516. https://doi.org/10.1126/science.1144004
Lohmann J, Ditlevsen PD (2021) Risk of tipping the overturning circulation due to increasing rates of ice melt. P Natl Acad Sci USA 118(9):e2017989118. https://doi.org/10.1073/pnas.2017989118
Ma J, Xu Y, Li Y, et al (2019) Predicting noise-induced critical transitions in bistable systems. Chaos 29(8). https://doi.org/10.1063/1.5115348
Mandal A, Sarkar S, Chakraborty S, et al (2025) Mitigating ecological tipping points via game–environment feedback. In: Proceedings A, The Royal Society, p 20240915
O'Keeffe PE, Wieczorek S (2020) Tipping phenomena and points of no return in ecosystems: beyond classical bifurcations. SIAM J Appl Dyn Syst 19(4):2371–2402. https://doi.org/10.1137/19M1242884
Oraby T, Thampi V, Bauch CT (2014) The influence of social norms on the dynamics of vaccinating behaviour for paediatric infectious diseases. P Roy Soc B-Biol Sci 281(1780):20133172. https://doi.org/10.1098/rspb.2013.3172
Pananos AD, Bury TM, Wang C et al (2017) Critical dynamics in population vaccinating behavior. P Natl Acad Sci USA 114(52):13762–13767. https://doi.org/10.1073/pnas.1704093114
Ritchie PD, Alkhayuon H, Cox PM et al (2023) Rate-induced tipping in natural and human systems. Earth Syst Dynam 14(3):669–683. https://doi.org/10.5194/esd-14-669-2023
Sarkar S, Narang A, Sinha SK et al (2021) Effects of stochasticity and social norms on complex dynamics of fisheries. Phys Review E 103(2):022401. https://doi.org/10.1103/PhysRevE.103.022401
Scheffer M, Bascompte J, Brock WA et al (2009) Early-warning signals for critical transitions. Nature 461(7260):53–59. https://doi.org/10.1038/nature08227
Scheffer M et al (1998) Ecology of shallow lakes, vol 1. Springer. https://doi.org/10.1007/978-1-4020-3154-0
Siteur K, Eppinga MB, Doelman A et al (2016) Ecosystems off track: rate-induced critical transitions in ecological models. Oikos 125(12):1689–1699. https://doi.org/10.1111/oik.03112
Smith JM (1982) Evolution and the Theory of Games. Cambridge University Press. https://doi.org/10.1007/978-1-4684-7862-4_22
Sun TA, Hilker FM (2020) Analyzing the mutual feedbacks between lake pollution and human behaviour in a mathematical social-ecological model. Ecol Complex 43:100834. https://doi.org/10.1016/j.ecocom.2020.100834
Suzuki Y, Iwasa Y (2009) The coupled dynamics of human socio-economic choice and lake water system: the interaction of two sources of nonlinearity. Ecol Res 24:479–489. https://doi.org/10.1007/s11284-008-0548-3
Wang R, Dearing JA, Langdon PG et al (2012) Flickering gives early warning signals of a critical transition to a eutrophic lake state. Nature 492(7429):419–422. https://doi.org/10.1038/nature11655
Weitz JS, Eksin C, Paarporn K et al (2016) An oscillating tragedy of the commons in replicator dynamics with game-environment feedback. P Natl Acad Sci USA 113(47):E7518–E7525
Wieczorek S, Xie C, Ashwin P (2023) Rate-induced tipping: Thresholds, edge states and connecting orbits. Nonlinearity 36(6):3238. https://doi.org/10.1088/1361-6544/accb37
Yang A, Wang H, Zhang T, et al (2022) Stochastic switches of eutrophication and oligotrophication: Modeling extreme weather via non-gaussian lévy noise. Chaos 32(4). https://doi.org/10.1063/5.0085560
Yang A, Wang H, Yuan S (2023) Tipping time in a stochastic leslie predator-prey model. Chaos Soliton Fract 171:113439. https://doi.org/10.1016/j.chaos.2023.113439
Yang A, Yuan S, Zhang T (2024) Environmental stochasticity driving the extinction of top predators in a food chain chemostat model. J Nonlinear Sci 34(3):50. https://doi.org/10.1007/s00332-024-10026-6
Zhang Z (1992) Qualitative theory of differential equations, vol 101. American Mathematical Soc